Aggregation and Self-Assembly of Hydrophobins from *Trichoderma reesei*: Low-Resolution Structural Models

Mika Torkkeli,* Ritva Serimaa,* Olli Ikkala,† and Markus Linder‡

*Department of Physics, University of Helsinki, FIN-00014, Helsinki, Finland; †Department of Engineering Physics and Mathematics, and Institute of New Materials, Helsinki University of Technology, FIN-02015 HUT, Espoo, Finland; ‡Technical Research Centre of Finland, VTT Biotechnology, FIN-02044 VTT, Finland

ABSTRACT Hydrophobins are secreted fungal proteins, which have diverse roles in fungal growth and development. They lower the surface tension of water, work as adhesive agents and coatings, and function through self-assembly. One of the characteristic properties of hydrophobins is their tendency to form fibrillar or rod-like aggregates at interfaces. Their structure is still poorly known. In a step to elucidate the structure/function relation of hydrophobin self-assembly, we present the low-resolution structure of self-assembled fibrils of the class II hydrophobin HFBII from *Trichoderma reesei* based on small and wide-angle x-ray scattering. We first studied the solution state (10 mg/mL) of both HFBI and HFBII and showed that they formed assemblages in aqueous solution, which have a radius of gyration of ~24 Å and maximum dimension of ~65 Å, corresponding to the size of a tetramer. This result was supported by size-exclusion chromatography. Undried samples of HFBII fibrils had a monoclinic crystalline structure, which changed to hexagonal when the material was dried. A low-resolution structure for the HFBII fibrils is suggested. There are data in the literature based on staining properties suggesting that hydrophobins of class I form assemblies with an amyloid structure. Comparison of the HFBII data (x-ray results, staining with thioflavin T) to published data showed that the HFBII assemblages are not amyloid.

INTRODUCTION

Hydrophobins form a group of proteins, which seem to be ubiquitous in filamentous fungi. They are fairly small (7–15 kDa) and are secreted. They have a wide range of functions in fungal growth and development, which mostly are linked to surface-chemical properties, such as lowering of surface tension and formation of various surface layers. Their role to lower the surface tension has been demonstrated by gene deletions, which result in suppression of aerial hyphae formation (Wösten et al., 1999). Hydrophobins, although not being toxins themselves, promote the infectivity of pathogenic fungi apparently through their adhesive and surface chemical properties (Ebbole, 1997). Often several different hydrophobins are found in a single species of fungi, each having specific roles during different stages of development and each being regulated separately (Nakari-Setälä et al., 1997; Wösten, 2001).

Another characteristic property of hydrophobins is that even when their primary sequences differ largely, they all share one common feature, that is, eight cysteine residues at specific locations. Consequently, disulfide bonds are formed leading to four loops, which in turn form two spatially separated pairs. Despite the low sequence similarity, hydropathy plots allow classification of hydrophobins into classes I or II (Wessels, 1994). On the primary structure level their main difference is in the second loop, which is longer and more hydrophobic for the class I hydrophobins. Biological studies have shown that some hydrophobins can partially complement each other (Kershaw et al., 1998; Wösten et al., 1999).

Hydrophobins are strongly surface active, leading to various forms of aggregation and self-assembly on surfaces and in solution. Class I hydrophobins, such as SC3 of *Schizophyllum commune*, are found to form a rodlet layer at interfaces (Wösten et al., 1993). Such aggregates are very stable and cannot be dissolved in detergents such as sodium dodecyl sulfate or most solvents except in some strong acids, e.g., trifluoroacetic acid. However, after the acid is evaporated, SC3 becomes soluble in water and can be repeatedly aggregated. For the class II hydrophobin, cerato-ulmin (Takai, 1974), microscopic needle-like aggregates have been described. They dissolve more easily in, for example, sodium dodecyl sulfate or ethanol.

Such fibrillar assembly of hydrophobins on surfaces suggests to consider whether they are in any way related to amyloid fibrils. The poorly soluble amyloid fibrils are rich in parallel-extended β-sheets (Rochet and Lansbury, 2000). More recently there have been several reports showing that the aggregates of class I hydrophobins fulfill many of the criteria for amyloid assemblies. For example de Vocht (de Vocht et al., 2000; de Vocht, 2001) showed that the dyes thioflavin T (ThT) and Congo red show the same spectroscopic changes together with SC3 and SC4 as they do with amyloid fibrils. It has also been shown that reduction of the cystines destabilized SC3 but that it retains its property to form amyloid-like rodlet structures even after reduction (de Vocht et al., 2000).

No three-dimensional structure has yet been presented for hydrophobins, and the already published studies suggest that there may not be a clearly defined solution structure at

Submitted February 1, 2002, and accepted for publication May 1, 2002.

Address reprint requests to Dr. M. Linder, Technical Research Centre of Finland, VTT Biotechnology, P.O. Box 1500, FIN-02044 VTT, Finland. Tel.: 358-9-4565136; Fax: 358-9-4552103; E-mail: markus.linder@vtt.fi.

0006-3495/02/10/2240/08 $2.00

all. In an NMR study, a core of β sheet structure was reported for class I hydrophobin EAS from *Neurospora crassa*, which otherwise was unstructured (Mackay et al., 2001). Our attempts to produce crystals for high-resolution structure determinations have been unsuccessful. Circular dichroism studies show that SC3 contains β-structure in solution but upon aggregation the α-helical content increases and then changes into a second β-conformation (de Vocht et al., 1998).

Very little is known about the structural features in hydrophobins and the molecular basis, which gives them their remarkable biophysical properties. Self-assembly seems to be a general property of hydrophobins and given that the biophysical properties are all in one way or the other linked to self-assembly, the relevant conclusions on the functionality can be made already by analyzing the structures at the length scales corresponding to the self-organization (Muthukumar et al., 1997), i.e., at the nanometer-scale, even if the full structural analysis has not yet been achieved. We noted in our work with the hydrophobins HFBI and HFBII from *Trichoderma reesei* that different types of assemblages can be seen by optical microscopy and that they are formed readily and set off by mixing or liquid handling. We extended this observation in this work using small angle x-ray scattering (SAXS) and wide-angle x-ray scattering (WAXS), as well as size-exclusion chromatography, to study the structure of the fibrils and the assemblages in solution.

MATERIALS AND METHODS

Purification of hydrophobins

Hydrophobins were purified essentially as in Linder et al. (2001) and Askolin et al. (2001). Briefly, HFBI was extracted from *T. reesei* strain VTT-D-98492 mycelium with 1% sodium dodecyl sulfate in 0.2 M sodium-acetate buffer, pH 5.0. Buffer exchange to 15 mM Tris, pH 9.0, buffer was then done by desalting on 10DG columns (BioRad, Hercules, CA). The sample was then loaded on a Resource Q column (Amersham Pharmacia Biotech, Uppsala, Sweden) and eluted with a linear salt gradient from 0 to 0.2 M NaCl. The HFBI peak fraction was then loaded onto a 1 $\times$ 20 cm Vydac C4 (Grace Vydac, Hesperia, CA) high performance liquid chromatography reversed phase column equilibrated with 0.1% trifluoroacetic acid and eluted with a linear gradient of acetonitrile with 0.1% trifluoroacetic acid. The HFBI peak fraction was finally lyophilized. HFBII was purified from the culture medium of a fermentation of *T. reesei* strain QM9414 by extraction with 2% of the nonionic surfactant Berol 523 (Akzo-Nobel, Sweden). The extracted fraction was further purified by high performance liquid chromatography as described above and then lyophilized. Lyophilization was in all cases continued for 20 h at 0.2 mbar and a final temperature of 20°C.

Formation of assemblages

Fibrillar assemblages of hydrophobins are formed easily by shaking in most hydrophobin solutions. A concentration of 7.5 mg/mL hydrophobin (HFBI or HFBII, lyophilized and dissolved) was used in 0.1 M acetate buffer, pH 5.0, with 20 mM $CuSO_4$ in a final volume of 0.9 mL. The solution was mixed on a laboratory shaker for 1 h and then centrifuged using 5000 $\times$ *g* for 5 min. The pellet was then characterized as such (subsequently denoted as the undried sample) or washed with 1 mL of water, pelleted again, and lyophilized as described above (subsequently denoted as the lyophilized sample).

Size-exclusion chromatography

The effective sizes of the hydrophobin complexes were determined by size-exclusion chromatography. A Superdex 75 column (Amersham Pharmacia Biotech, Uppsala, Sweden) was run on an Äkta explorer chromatography equipment (Amersham Pharmacia Biotech, Uppsala, Sweden) using 50 mM acetate buffer, pH 5, with 0.2 M NaCl and a flow-rate of 0.5 mL/min. Molecular weight standards were: ovalbumin (43 kDa), cytochrome C (12.4 kDa), aprotinin (6.5 kDa), and vitamin B12 (1.4 kDa). All were obtained from Sigma and used at a concentration of 1 mg/mL. Lyophilized samples of HFBI and HFBII were dissolved in water to a concentration of 10 mg/mL or 0.5 mg/mL. The injection volume was 100 μL in all cases.

X-ray scattering experiments of undried or lyophilized HFBI and HFBII fibrils

The solid fibrillar samples were measured using SAXS and WAXS with a sealed Cu anode x-ray tube used in the point focusing mode. The CuK_α radiation (λ = 1.542 Å) was monochromatized with a Ni-filter and a glass mirror. The scattering was detected with a one-dimensional linear proportional counter (M-Braun OED-50). A small amount of the fibrils was placed in a sample cell, which consisted of two polyimide films supported by a flat steel ring and two cover plates. The cell was filled with a drop of distilled water, and the ring and the films were screwed tightly with the cover plates to prevent drying. The data were collected in two parts. In the SAXS measurement, the distance between the sample and the detector was 160 mm and the measured range of *k*-values was 0.03 to 0.5 1/Å where the length of the scattering vector is defined by $k = (4\pi/\lambda)\sin\theta$, in which 2θ = the scattering angle. In the WAXS measurement, the detector was tilted ~10°. The sample-to-detector distance was reduced to ~100 mm, and the second range of *k* values was 0.5 to 2.5 1/Å. The lyophilized nonassembled solid samples were measured for 15 h and 1.5 h at the small and wide angles, respectively. The undried samples were measured in 3- or 6-h intervals to monitor any changes in the structure due to sample drying. The measurement at small angles showed very little variation in the intensities of the reflections and 18 h of data were accepted. In the wide-angle scattering measurement, there were signs of loss of water, and only first 6 h of data are accepted.

SAXS measurement of HFBI and HFBII in solution

The aggregation in solution was studied using SAXS with the same equipment that was used for the solid samples. However, line focusing was used to increase the intensity and the instrumental function had a full-width half-maximum of 0.005 1/Å and 0.35 1/Å in horizontal and vertical directions, respectively. The sample cell was a larger variant of the type described above. The sample was injected with a syringe, and the syringe hole was hermetically glued. The measurements were made at 25°C and 80°C for 240 and 90 min, respectively. The background due to the solvent was measured separately and subtracted from the intensity curves of the samples. The concentration of protein was 10 mg/mL in all experiments.

Thioflavin T staining

Staining with ThT was performed essentially as described in de Vocht et al. (2000) and Butko et al. (2001) using fluorescence spectroscopy. The excitation wavelength was 435 nm, and the emission spectra were monitored between 450 and 600 nm. Samples consisting of 50 mM glycine/

NaOH, pH 8.5, buffer containing 5 μM ThT (Sigma) were used with or without 67 μg/mL HFBI or HFBII. The spectra were measured for control samples consisting of the buffer alone, the buffer containing ThT, or the hydrophobin. The combination of ThT and hydrophobins was measured either by first adding the hydrophobin, which was "preassembled" by vortexing for 1 min, and then adding ThT, or by adding hydrophobin to a ThT solution. A Shimadzu RF-5000 spectrofluorometer was used for the measurements.

RESULTS

Formation of the fibrillar aggregates on the surfaces

Both HFBI and HFBII form fibrils on surfaces, which can be seen in an optical microscope. Fig. 1 *A* shows a dark-field microscope image of clustered needle-like aggregates of HFBII on an air bubble after an intensive mixing of the sample and Fig. 1 *B* depicts isolated fibrils formed during a more gentle mixing. In the latter case, the fibrils are more regular in size and shape with diameters of 2 to 3 μm and lengths of 15 to 25 μm. In some cases needles up to several hundred micrometers were observed. The HFBII fibrils were collected by centrifugation for x-ray scattering studies, and they were characterized either as such (undried) or after drying (lyophilized). HFBI also formed aggregates upon mixing, but they were of less regular shape (Fig. 1 *C*). They were more unstable than those of HFBII and dissolved during standing. Therefore, we did not manage to collect HFBI fibrils by centrifugation and study them by x-ray scattering.

Structural studies of undried and lyophilized HFBI and HFBII

Fig. 2 *A* depicts the x-ray diffraction pattern of the undried HFBII fibrils, showing several sharp diffraction peaks. The measurement with another sample gave almost identical positions and intensities for the principal reflections. This suggests that the current data refer to a single crystal structure and that the reflection intensities are not affected by the sample texture. The first four reflections can be indexed according to a monoclinic crystal structure with a unique axis c. Due to the overlap of the reflections, it is not possible to determine the space group solely based on the data in Fig. 2 *A*. Only three monoclinic space groups (numbered as 3–5) were considered, the other 12 being excluded because they possess mirror symmetry (Hahn, 1983). The lattice constants for the space group 3 (full Hermann-Mauguin symbol *P 1 1 2)* are $a = 38.0$ Å, $b = 46.6$ Å, $c = 27.9$ Å, $\gamma = 122°$, and the volume of the unit cell is 41,040 Å^3. The constants for the group 4 ($P\ 1\ 1\ 2_1$) are $a = 38.0$ Å, $b = 46.6$ Å, $c = 55.8$ Å, $\gamma = 122°$. Therefore, the length c and thus also the volume of the cell is doubled. Because space group 5 would produce reflections at lower k values than the presently observed first peak, we prefer groups 3 and 4. The average size of crystallites was estimated from the widths of the reflections by using the well-known Scherrer formula. The effect of the instrumental broadening on the width of the reflections was taken into account by assuming that the

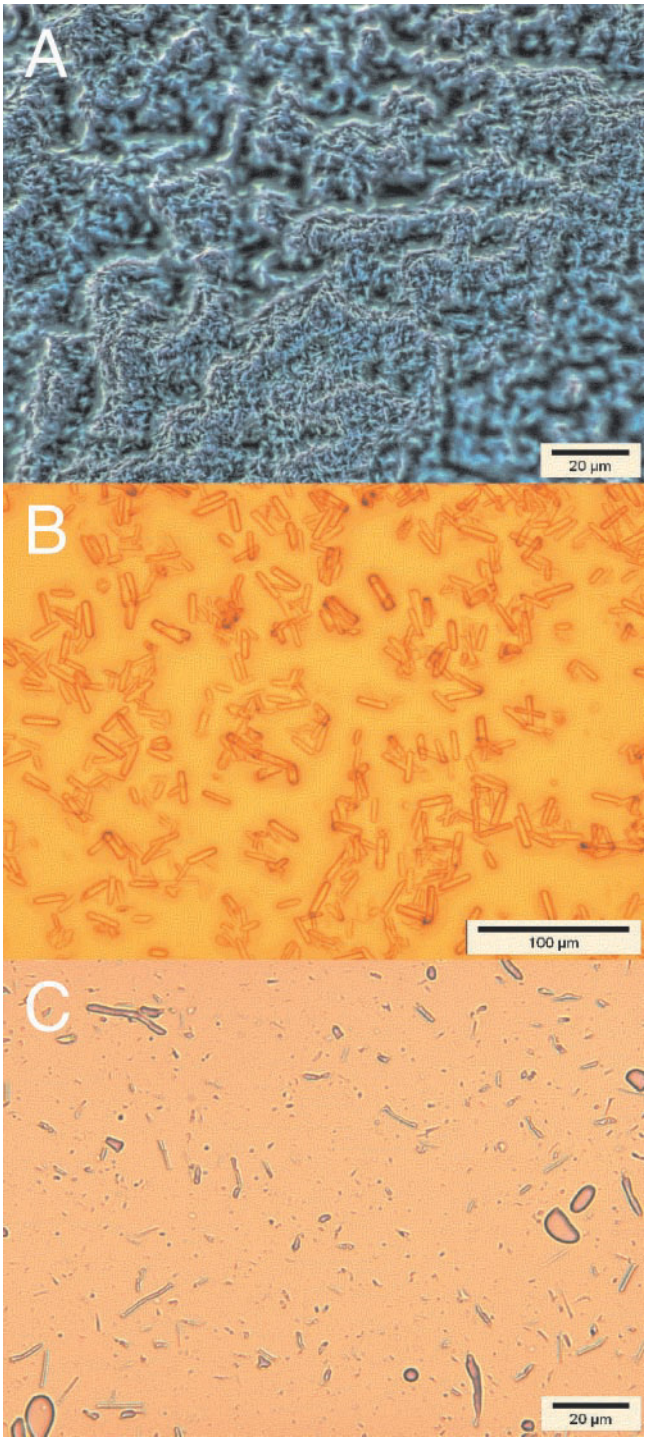

FIGURE 1 (*A*) Set of aggregates due to HFBII formed on an air bubble due to extensive shaking of the sample. (*B*) More gentle mixing renders distinct HFBII fibrils of more regular shape. (*C*) Fibrils observed for HFBI are not as well defined as for HFBII and are more fragile.

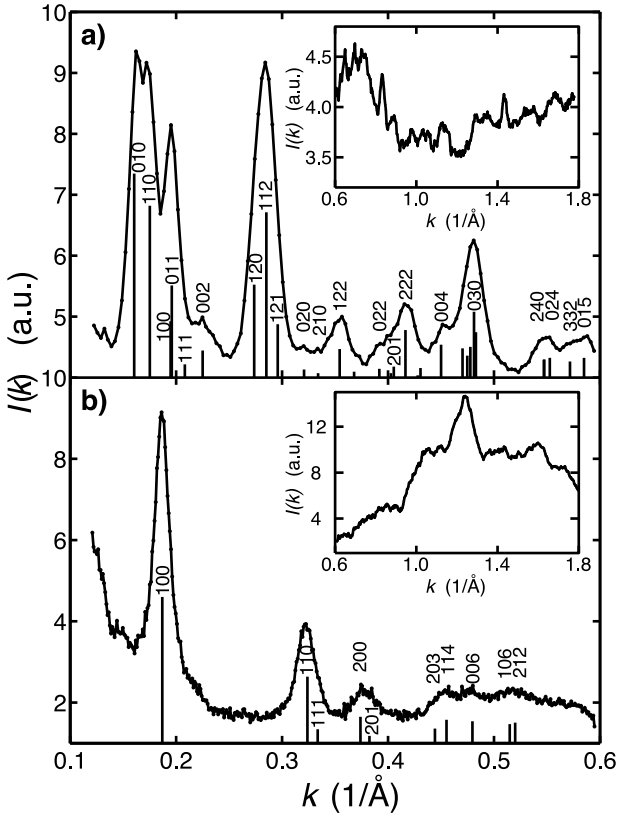

FIGURE 2 Scattering intensities of the HFBII fibrils: (*A*) Undried sample showing a monoclinic structure, the reflections are indexed according to monoclinic space group 4. (*B*) Dried sample showing a hexagonal arrangement.

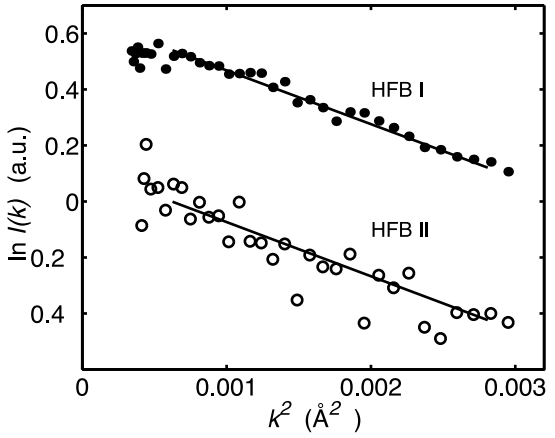

FIGURE 3 SAXS intensity curves at low angles for HFBI and HFBII in the aqueous solutions at concentration 10 mg/mL at 25°C, suggesting scattering from well defined particles. Solid lines represent Guinier-law behavior corresponding to R_g = 24 Å.

shapes of both the reflection and the instrumental function are approximately Gaussians (Balta-Calleja and Vonk, 1989). Because the reflections are overlapping, only the size range 450 to 900 Å is given.

Referring to the crystal structures in the Protein Data Bank (Berman et al., 2000), it is evident that monoclinic crystals whose asymmetric group contains one or two protein chains of comparable size, have protein densities between ≥0.59 g/cm and ≥0.97 g/cm. Thus, the cell with a volume of 41,040 Å^3 is expected to contain 2 to 3 HFBII monomers (each 7171 Da). On the other hand, when there are three chains (as well as in the case of hexagonal structures) the protein densities are lower, ~≥0.5 g/cm or less. Therefore, we suggest that the asymmetric unit contains one monomer if the space group 3 is selected, or two monomers in the case of space group 4. The protein density is ≥0.58 g/cm in both cases and therefore the water content is ~45 wt%. This is in the range commonly observed for protein crystals (Matthews, 1968). A possible low-resolution structure is shown below (see Fig. 7).

Fig. 2 *B* shows the diffraction pattern of the dried HFBII fibrils, i.e., after lyophilization. Below the shown regime at $k < 0.08$ 1/Å, the intensity curve increases strongly toward the zero scattering angle, and the intensity $I(k)$ obeys a power law $k^{-3.8}$. This scattering might arise from voids in the sample (Glatter and Kratky, 1982). The first three reflections are located at $k^* = 0.188$ Å^{-1}, $\sqrt{3}\ k^*$, and 2 k^* and agree well with a two-dimensional hexagonal arrangement. The unit cell parameters are $a = b = 38.8$ Å, i.e., comparable with the monoclinic form. However, some of the observed higher order reflections do not agree with a two-dimensional hexagonal lattice and we suggest a three-dimensional crystal structure even in this case. We consider the space groups 169 through 172 (*P6_1*, *P6_5*, *P6_2*, or *P6_4*) (Hahn, 1983). In keeping with the previous density, the *c* axis is now increased to ~80 Å because the hexagonal structure has a sixfold symmetry (instead of twofold symmetry) around the unique axis. The indexation in Fig. 2 *B* is based on the space group 169 (*P6_1*) with $a = b = 38.8$ Å and $c = 78$ Å. For the dried sample, the average size of the crystallites was slightly lower than for the undried sample, ~400 Å.

The high performance liquid chromatography purified and lyophilized HFBI was only weakly ordered in the solid state. Its intensity curve was typical to amorphous materials and contained no sharp diffraction peaks.

Aqueous solutions of HFBI and HFBII

The SAXS intensities of 10 mg/mL aqueous solutions of HFBI and HFBII resemble each other closely (Fig. 3) at small k (for $k < 0.06$ 1/Å). Both obey the Guinier approximation, i.e., $I(k) \sim \exp(-\frac{1}{3}\ k^2R_g^2)$, in which R_g is the radius of gyration of the scattering particles, indicating that there are individual dissolved objects (Glatter and Kratky, 1982). The intensities were corrected for the instrumental effects, and the distance distribution functions were calculated using the indirect transform program GNOM (Svergun et al.,

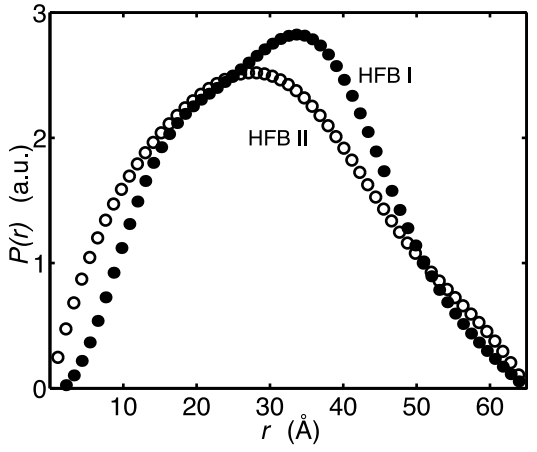

FIGURE 4 Distance distribution functions for HFBI and HFBII in aqueous solution at the concentration of 10 mg/mL at 25°C.

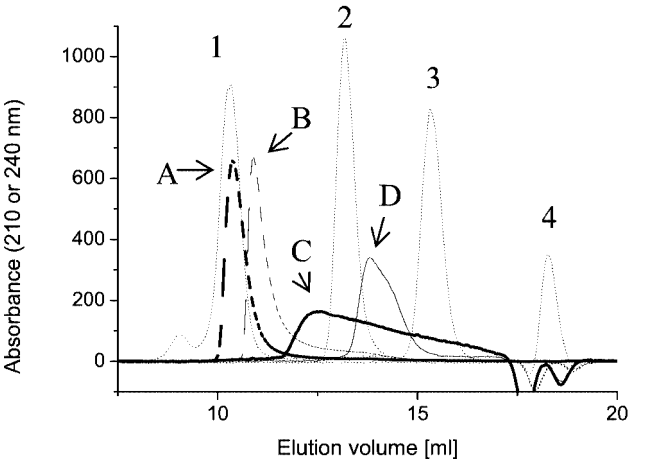

FIGURE 5 Size-exclusion chromatography showing that both HFBI and HFBII are multimeric complexes (putatively tetramers) at high concentrations. The HFBI sample at 10 mg/mL is shown as a thick segmented line (*A*) and the HFBI sample at 0.5 mg/mL as a thick solid line (*C*). The HFBII sample at 10 mg/mL is a thin segmented line (*B*) and HFBII at 0.5 mg/mL is a thin solid line (*D*). The standards are shown as thin dotted lines (*1* = 43 kDa, *2* = 12.4 kDa, *3* = 6.5 kDa, *4* = 1.4 kDa). The data show that HFBI forms slightly larger complexes than HFBII and that the HFBI complex is more associated at low concentration possibly forming a dimer.

1994). The determined radii of gyration were 24 Å for both HFBI and HFBII. The distance distribution functions (compare with Fig. 4) of HFBI and HFBII indicate that the particles in both samples have a maximum dimension of ~65 Å. The values are larger than one would expect on the basis of the mass of the monomers. The volumes of the monomers may be estimated as 9500 $Å^3$and 9200 $Å^3$ for HFBI and HFBII, respectively, based on standard residue volumes (Pontius et al., 1996). The volume of the scattering particles may be estimated from the ratio of the scattering at zero angle $I(0)$ and the so-called scattering invariant Q (Glatter and Kratky, 1982) by $V = 2\pi^2 I(0)/Q$. This analysis is rather sensitive to any residual background in the intensities and therefore the relative errors are quite large. Currently, we obtain (51,000 ± 8000) $Å^3$ and (38,000 ± 10,000) $Å^3$ for HFBI and HFBII, respectively. The solution SAXS results suggest that for both HFBI and HFBII well-defined aggregates are formed consisting of several protein chains. The SAXS intensity curves were almost identical at temperatures 25°C and 80°C, indicating that the aggregates are stable at this temperature range and concentration.

Size-exclusion chromatography

Size-exclusion chromatography confirmed that both HFBI and HFBII are aggregated in solution (Fig. 5). When injecting the samples at 10 mg/mL, HFBI eluted as a 35-kDa peak and HFBII as a 30-kDa peak. The calculated tetramer size is 30 kDa for HFBI (monomer 7.54 kDa) and 28 kDa for HFBII (monomer 7.2 kDa). When injecting the sample at 0.5 mg/mL both hydrophobins eluted later. HFBI eluted as a broad skew peak with the maximum corresponding to a 16-kDa protein and HFBII as a 8-kDa protein. Thus, there seems to be an equilibrium between the components of the putative tetramer, which exists at high concentrations and probably monomers in the case of HFBII and dimers in the case of HFBI.

Thioflavin T staining

In all samples containing hydrophobin, vortexing caused assembly of the proteins as seen by the appearance of sharp scattering peak of the excitation light. No change in fluorescence intensity of the ThT could, however, be observed in any of the samples containing assembled or nonassembled hydrophobins.

DISCUSSION

During studies and purification of the hydrophobins HFBI and especially HFBII (Linder et al., 2001), we noted that both have a high tendency to form aggregates of fibrillar appearance. Depending on the preparation conditions, their length varied from few to hundreds of micrometers. The hydrophobins HFBI and HFBII have properties common to this group of proteins, such as high surface activity and a high propensity to adhere to surfaces (Linder et al., 2002).

We have previously noted that hydrophobins can be purified by extraction with nonionic surfactants (Linder et al., 2001), a method commonly used for poorly soluble membrane proteins. The affinity of hydrophobins to the surfactant phase is structure dependent because reduction and unfolding causes a total loss of partitioning to the surfactant phase.

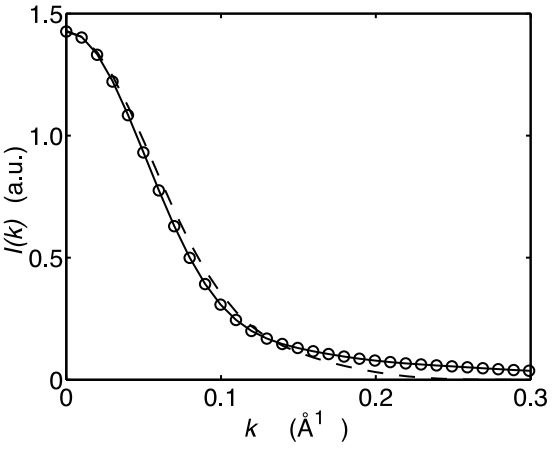

FIGURE 6 Experimental solution scattering intensity (*circles*) for HFBII, corrected for the instrumental effects. The solid curve is the low-resolution ab initio model obtained by the program DAMMIN. The dashed curve represents the intensity of one tetramer from the combined fitting of the scattering data from both solution and crystalline samples.

We found that the lyophilized HFBI and HFBII hydrophobins were easily dissolved in water to a concentration of at least 20 mg/mL. However, their hydrophobic/amphiphilic nature suggests aggregation in solution, and in fact we observe that both HFBI and HFBII exist as rather well-defined aggregates consisting of a few chains as shown in Figs. 4 and 5 based on SAXS and size-exclusion chromatography. SAXS shows that the soluble entities have a relatively large radius of gyration of ~24 Å and the maximum dimension ~65 Å. Dimers of comparable chain length typically render a value R_g = 15 to 18 Å, which, therefore, is considerably smaller (see e.g., Brayer and McPherson, 1983; Bally and Delettre, 1989). However, two such dimers displaced by the appropriate transformation related to the *P 1 1 2₁* space group yields approximately R_g = 23 Å, which would suggest that the entities in solution as shown in Figs. 3 and 4 are actually tetramers. In the size-exclusion chromatography (Fig. 5) tetramers are also observed at the same concentration 10 mg/mL but at lower concentrations additionally dimers and even monomers are observed. A clearly different result was obtained in a previous study where it was reported that the hydrophobin EAS from *N. crassa* exists as monomers in sedimentation equilibrium experiments (Mackay et al., 2001).

The collection and x-ray characterization of the fibrils was only successful for HFBII because the HFBI fibrils were fragile and dissolved upon standing. According to the x-ray scattering analysis, the undried fibrils of HFBII have a monoclinic structure, and they are more crystalline than the lyophilized fibrils, which have a hexagonal structure. The difference is probably due to the additional hydrogen bonds of the added water molecules.

As was pointed out in the introduction, very little is presently known of the three-dimensional structure of hydrophobins. To assess the refined complete crystalline structure of the fibrils, alignment techniques are clearly needed preferably in conjunction with synchrotron radiation studies. Meanwhile, we have further analyzed the HFBII SAXS data of both the solution and the undried fibril states (Figs. 2 *A*, 3, and 4) using common low-resolution models. At present, such models remain speculative and their relation to the actual structure remains open. First, a structural model for HFBII in solution was restored from the solution SAXS intensity curve at $0.02 < k < 0.3$ 1/Å by using the program DAMMIN (Svergun, 1999). The program builds the scattering unit from dummy particles and simulated annealing is used to find a configuration that best fits to the measured SAXS data. Fig. 6 shows the fitted intensity together with the experimental intensity of HFBII. The root-mean square deviation to the raw experimental data was 2.19. The resulting solution structure is slightly elongated (Fig. 7 *A*). The shape interestingly reveals four "branches," which could be a visualization of the aggregation into tetramers. No a priori assumptions were made in the fitting, and therefore, the fitted shape is a further evidence of aggregation into tetramers at high concentrations.

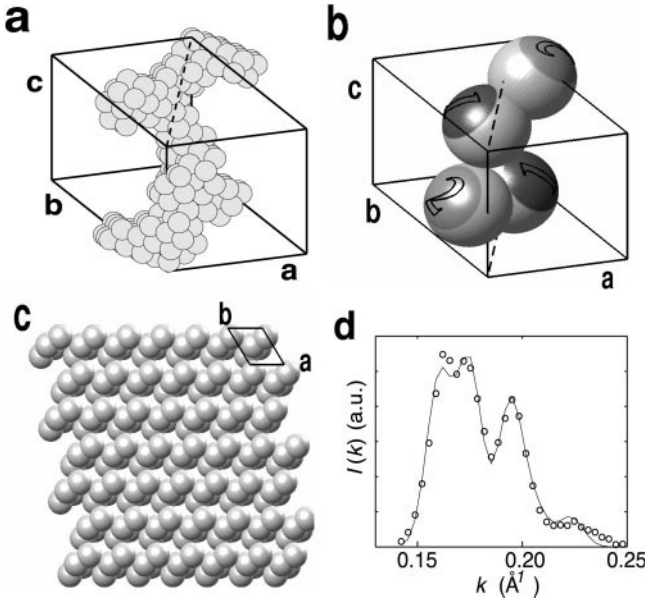

FIGURE 7 (*A*) Low-resolution model for HFBII explaining the solution SAXS intensity. The model supports the hypothesis that the scattering particles are well-defined tetramers at the concentration of 10 mg/mL. To facilitate comparison with the corresponding crystalline models, the aggregate has been plotted in a monoclinic unit cell. (B) Repeat unit of a low-resolution model of a correct symmetry that explains the SAXS data of the undried HFBII fibrils. The two monomers in the asymmetric unit (labeled *1* and *2* in *B*) constitute a dimer, and the second dimer (similarly marked) is obtained from the first by a 180° rotation around the *c* axis and translation by c/2. (*C*) Stacking of the repeat units, showing the monoclinic arrangement of void spaces, filled with water molecules. (*D*) Quality of fitting to the scattering intensity of the undried fibrils presented in Fig. 2 *A* at small values of the magnitude of the scattering vector *k*.

A so far tentative hypothesis was laid that in the fibrillation the tetrameric aggregates observed in the solution would become stacked to form the crystallites within the fibrils. Second, it was studied whether the solution tetramers essentially of the shape shown in Fig. 7 *A* could be packed in the monoclinic crystalline lattice to produce the diffraction data of the undried HFBII fibrils (Fig. 2 *A*). As suggested by Fig. 7 *A* and modified by the required crystal symmetry (Fig. 2 *A*), each HFBII monomer was crudely approximated as an identical spherical unit of radius 16 Å, and the space group 4 was chosen for the crystal structure. The model was fitted simultaneously to the experimental scattering intensity of the fibrils in the range $0.14\ \text{Å}^{-1} < k < 0.25\ \text{Å}^{-1}$ and the experimental distance distribution function obtained from the solution SAXS measurement (Fig. 4). The fitting suggested packing of the proteins somewhat diagonally within the unit cell (Fig. 7 *B*). Further note that the models shown in Fig. 7, *A* and *B* are grossly of similar shape. To illustrate more clearly the crystalline structure of Fig. 7 *B*, the packing is shown in Fig. 7 *C* along the *c* axis. Taken the suggested water concentration as discussed before, it is expected that the vacancies illustrated are the water channels filling approximately one-half of the volume. Finally, Fig. 7 *D* illustrates the very good fit achieved to the fibrillar SAXS intensity curve of the data of Fig. 2 *A*. Similarly, Fig. 6 shows that the model fits well with the solution SAXS data.

It is not easy to expect that it would be purely fortuitous that the tetramers observed in the concentrated solutions would explain the essential features of the monoclinic crystalline structure of the fibrils. Note that such solution state tetramers were observed to be stable as they tolerated heating to 80°C. This may give hints to understand the mechanisms for the fibrillation. Generally, strongly amphiphilic molecules should have a small critical aggregation concentration. Therefore, starting from a low concentration of HFBII, aggregation into dimers is first observed and upon increasing the concentration, mostly stable tetramers are observed. Upon further enriching the concentration, e.g., on surfaces, the higher aggregates may be unstable in solution and formation of the fibrils may be therefore triggered.

Self-assembly has been suggested to play a major role in the function of hydrophobins. This is most evident in the case of the rodlet layer that is formed by some class I hydrophobins. Careful measurements have shown that the SC3 hydrophobin undergoes major conformational changes during rodlet layer formation and at the air/water interface (de Vocht et al., 1998). Although it is not clear how self-assembly of HFBI and HFBII would relate to their high surface activity and tendency to adhere to surfaces, the observed easy formation of microscopic fibrils suggests that they easily self-assemble.

Finally, a possible connection to the amyloid fibers is contemplated. Recently, it has been reported that some class I hydrophobins can be stained by the characteristic stains, ThT and Congo red, which typically react with amyloid fibrils (de Vocht et al., 2000; de Vocht, 2001; Mackay et al., 2001; Butko et al., 2001) suggesting that the hydrophobins fibrils could be classified to be functional amyloid fibrils. However, in the amyloid structures the fibrils are unbranched and very thin, i.e., 70 to 130 Å in diameter and they are composed of several protofibrils, whose diameter is 25 to 35 Å (Serpell et al., 2000). In the case of transthyrethin, the diameter of the protofibrils is proposed to be 54 Å (Lazo and Downing, 1998). The protofibrils are composed of polypeptide chains that are in the cross-β-conformation. The β-strands are perpendicular to the fiber axis, and a reflection arising from the regular 4.7 Å separation of successive β-strands along the axis of the protofibril dominates the x-ray diffraction pattern (Sunde and Blake, 1997). In studies of class I hydrophobin rodlets it has been estimated that the rodlet diameters range from 2 to 15 nm (Kershaw et al., 1998; Wösten et al., 1993; Lugones et al., 1998), which is also within the range of some other amyloid proteins. We tested in this work if HFBI and HFBII react with ThT, but we failed to see any effect, which is in contrast to typical amyloid behavior. This result is supported by the x-ray data where the diffraction patterns of the undried, and lyophilized HFBII fibrils indicate that the crystallites are quite large in all directions, not only along the fiber axis. No reflection corresponding to 4.7-Å spacing is observed, indicating that there is no well-ordered cross-β structure in the fibrils.

Our data show the main structural features of the assembled form of HFBII and the solution association of both hydrophobins. We are, however, unable to draw direct conclusions of how the assembly into fibrils is related to the function of hydrophobins. It will be interesting to see if comparable studies on class I hydrophobins reveal similar features. This seems likely at least on the protofilament level, indicated by superficial similarities in images obtained by atomic force microscopy and electron microscopy. It remains still a challenge to understand whether the fibrillation or rodlet formation is essential for the surface modification of the surface energies, such as, e.g., in the nanostructured surfaces within superhydrophobicity.

The Academy of Finland is thanked for financial support. Riitta Suihkonen is thanked for technical assistance.

REFERENCES

Askolin, S., T. Nakari-Setälä, and M. Tenkanen. 2001. Overproduction, purification, and characterization of the *Trichoderma reesei* hydrophobin HFBI. *Appl. Microbiol. Biotechnol.* 57:124–130.

Bally, R., and J. Delettre. 1989. Structure and refinement of the oxidized P21 form of uteroglobin at 1.64 A resolution. *J. Mol. Biol.* 206:153–170.

Balta-Calleja, F. J., and C. G. Vonk. 1989. X-Ray Scattering of Synthetic Polymers. Elsevier, Amsterdam.

Berman, H. M., J. Westbrook, Z. Feng, G. Gilliland, T. N. Bhat, H. Weissig, I. N. Shindyalov, and P. E. Bourne. 2000. The protein data bank. *Nucleic Acids Res.* 28:235–242.

Brayer, G. D., and A. McPherson. 1983. Refined structure of the gene 5 DNA binding protein from bacteriophage fd. *J. Mol. Biol.* 169:565–596.

Butko, P., J. P. Buford, J. S. Goodwin, P. A. Stroud, C. L. McCormick, and G. C. Cannon. 2001. Spectroscopic evidence for amyloid-like interfacial self-assembly of hydrophobin Sc3. *Biochem. Biophys. Res. Commun.* 280:212–215.

de Vocht, M. 2001. Structural Changes that Accompany the Self Assembly of Hydrophobins. Ph.D. Thesis. University of Groningen, Groningen.

de Vocht, M. L., I. Reviakine, H. A. Wosten, A. Brisson, J. G. Wessels, and G. T. Robillard. 2000. Structural and functional role of the disulfide bridges in the hydrophobin SC3. *J. Biol. Chem.* 275:28428–28432.

de Vocht, M. L., K. Scholtmeijer, E. W. van der Vegte, O. M. de Vries, N. Sonveaux, H. A. Wosten, J. M. Ruysschaert, G. Hadziloannou, J. G. Wessels, and G. T. Robillard. 1998. Structural characterization of the hydrophobin SC3, as a monomer and after self-assembly at hydrophobic/hydrophilic interfaces. *Biophys. J.* 74:2059–2068.

Ebbole, D. J. 1997. Hydrophobins and fungal infection of plants and animals. *Trends Microbiol.* 5:405–408.

Glatter, O., and O. Kratky. 1982. Small Angle X-Ray Scattering. Academic Press, New York, NY.

Hahn, T. 1983. IUCR International Tables of Crystallography. D. Reidel Publishing Company, Dordrecht, The Netherlands.

Kershaw, M. J., G. Wakley, and N. J. Talbot. 1998. Complementation of the mpg1 mutant phenotype in *Magnaporthe grisea* reveals functional relationships between fungal hydrophobins. *EMBO J.* 17:3838–3849.

Lazo, N. D., and D. T. Downing. 1998. Amyloid fibrils may be assembled from β-helical protofibrils. *Biochemistry.* 37:1731–1735.

Linder, M., K. Selber, T. Nakari-Setälä, M. Qiao, M.-R. Kula, and M. Penttilä. 2001. The hydrophobins HFBI and HFBII from *Trichoderma reesei* showing efficient interactions with nonionic surfactants in aqueous two-phase systems. *Biomacromolecules.* 2:511–517.

Linder, M., G. R. Szilvay, T. Nakari-Setälä, H. Söderlund, and M. Penttilä. 2002. Surface adhesion of fusion proteins containing the hydrophobins HFBI and HFBII from *Trichoderma reesei. Protein Sci.* 11:2257–2266.

Lugones, L. G., H. A. Wosten, and J. G. Wessels. 1998. A hydrophobin (ABH3) specifically secreted by vegetatively growing hyphae of *Agaricus bisporus* (common white button mushroom). *Microbiology.* 144: 2345–2353.

Mackay, J. P., J. M. Matthews, R. D. Winefield, L. G. Mackay, R. G. Haverkamp, and M. D. Templeton. 2001. The hydrophobin EAS is largely unstructured in solution and functions by forming amyloid-like structures. *Structure.* 9:83–91.

Matthews, B. W. 1968. The solvent content of protein crystals. *J. Mol. Biol.* 33:491–497.

Muthukumar, M., C. K. Ober, and E. L. Thomas. 1997. Competing interactions and levels of ordering in self-organizing polymeric materials. *Science.* 277:1225–1232.

Nakari-Setälä, T., N. Aro, M. Ilmen, G. Munoz, N. Kalkkinen, and M. Penttila. 1997. Differential expression of the vegetative and spore-bound hydrophobins of *Trichoderma reesei*– cloning and characterization of the hfb2 gene. *Eur. J. Biochem.* 248:415–423.

Pontius, J., J. Richelle, and S. J. Wodak. 1996. Deviations from standard atomic volumes as a quality measure for protein crystal structure. *J. Mol. Biol.* 264:121–136.

Rochet, J.-C., and P. T. Lansbury. 2000. Amyloid fibrollogenesis: themes and variations. *Curr. Opin. Struct. Biol.* 10:60–68.

Serpell, L. C., C. C. Blake, and P. E. Fraser. 2000. Molecular structure of a fibrillar Alzheimer's A β fragment. *Biochemistry.* 39:13269–13275.

Sunde, M., and C. Blake. 1997. The structure of amyloid fibrils by electron microscopy and x-ray diffraction. *Adv. Protein Chem.* 50:123–159.

Svergun, D. I. 1999. Restoring low- resolution structure of biological macromolecules from solution scattering using simulated annealing. *Biophys. J.* 76:2879–2886.

Svergun, D. I. and J. S. Pedersen. 1994. Propagating errors in small-angle scattering data treatment. *J. Appl. Cryst.* 27:241–248.

Takai, S. 1974. Pathogenicity and cerato-ulmin production in *Ceratocystis ulmi. Nature.* 252:124–126.

Wessels, J. G. H. 1994. Developmental regulation of fungal cell wall formation. *Annu. Rev. Phytopathol.* 32:413–437.

Wösten, H. A., M. A. van Wetter, L. G. Lugones, H. C. van der Mei, H. J. Busscher, and J. G. Wessels. 1999. How a fungus escapes the water to grow into the air. *Curr. Biol.* 9:85–88.

Wösten, H. A. B. 2001. Hydrophobins: multipurpose proteins. *Annu. Rev. Microbiol.* 55:625–646.

Wösten, H. A. B., O. M. H. de Vries, and J. G. H. Wessels. 1993. Interfacial self-assembly of a fungal hydrophobin into a rodlet layer. *Plant Cell.* 5:1567–1574.